RESEARCH

Torsional vibration characteristics analysis and vibration suppression research of compressor flexible rotor system considering fit clearance

Jie Wang[1] · Zhiqiang Huang[1] · Tao Li[1] · Gang Li[1] · Yuxing Duan[1] · Guoxu Zhang[1]

Abstract

Shale gas reciprocating compressors are usually faced with problems such as wide working conditions, multiple wells, and variable loads, which makes the torsional vibration of the compressor crankshaft serious. In addition, there is an inevitable fit clearance between the moving pairs of the shafting, which will increase the torsional amplitude value of the shafting and amplify the resonance risk. This paper presents a torsional vibration calculation method and a torsional vibration suppression technique for reciprocating compressor crankshaft systems, considering the influence of fit clearance and flexibility. A rigid-flexible coupling dynamic model of compressor crankshaft system that considers crosshead pin clearance is established by combining multibody dynamics, collision dynamics, and finite element method. The torsional angular displacement, angular velocity, and force characteristics of the compressor crankshaft system, considering fit clearance and part flexibility, are solved and analyzed. Additionally, the dynamic characteristics of the sliding bearings are determined by considering their clearance, using the finite difference method and the pressure disturbance method. A finite element model of the compressor crankshaft system considering the mixed clearances is constructed. The torsional vibration characteristics of the compressor crankshaft system are compared and analyzed under different fit clearances. The accuracy of the proposed model is validated through compressor on-site operation experiments. The speed error between the experimental and simulated results is found to be only 1.2%. Finally, research on clearance configuration optimization is conducted. The results demonstrate that with a crosshead pin clearance of 0.07 mm and a sliding bearing clearance of 0.1 mm, the angular displacement amplitude of the shafting is reduced by 1.76%, the peak value of rubbing is decreased by 29.49%, and the resonance point of the crankshaft system is minimized. This research offers theoretical guidance for ensuring the stable and reliable operation of compressors.

✉ Z. Huang
huangzq@swpu.edu.cn

[1] Southwest Petroleum University, No.8 Xindu Avenue, Chengdu, Sichuan, 610500, P.R. China
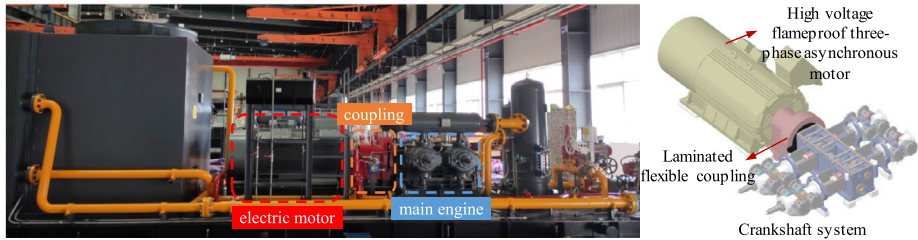
Springer

Fig. 1 Reciprocating compressor main engine

1 Introduction

The crankshaft system of reciprocating compressors is characterized by inherent flexibility and unavoidable clearances between the connecting components, as shown in Fig. 1. These clearances can exacerbate torsional vibration issues in the shafting, increasing the risks of bearing wear, bolt loosening, and even shaft fractures. Moreover, they also have an impact on the operational efficiency of the compressor and the safety of personnel. Consequently, it is crucial to investigate the effects of flexibility and clearance on the torsional vibration of crankshaft systems to ensure secure and stable compressor operation.

So far, research on considering hinged clearance in kinematic pairs has predominantly focused on the contact dynamics of planar mechanisms [1–6] and three-dimensional cylindrical hinged clearance [7–10]. For instance, Zhao et al. [11] investigated the joint clearance in robot manipulators, constructing dynamic equations for systems with clearance and accounting for friction effects using Coulomb friction. Their findings indicated that clearance led to increased joint contact forces, thereby impacting the accuracy of manipulator control systems. The research of Zhang et al. [12] suggested that smaller loads, moderate speeds, and simpler trajectories contributed to ensuring the stable operation of the mechanism. Chen et al. [13] employed ADAMS software to develop a dynamic model of a high-speed press transmission system that considered actual characteristics, including contact and friction. Their study confirmed that the influence of clearance on the mechanism's dynamic characteristics cannot be neglected. Similarly, Yan et al. [14] constructed a dynamic model of a four-bar mechanism accounting for three-dimensional rotating clearance joints. Their research shed light on the relative motion characteristics and nonlinear dynamic responses exhibited by misaligned shaft holes. Using the continuous contact law, Chen et al. [15] developed a dynamic model for a planar multibody system with clearance joints, focusing on the impact of dynamic characteristics on a crank-slider system with two clearance joints. Bai et al. [16] investigated the influence of mixed clearance, including axial clearance and rotational joint clearance in spatial and translational joints, on the dynamic response of planar mechanical systems using the crank-slider mechanism as the research subject. Their findings highlighted that mixed clearance had the most significant influence on the dynamic characteristics of the structure, with experimental validation supporting the accuracy of the research approach. The above research does not consider the influence of mechanism flexibility on the dynamic response of the system.

Furthermore, some scholars have explored the effects of bearing clearance on shafting dynamics [17–19]. Xu et al. [20] proposed a multibody system dynamic modeling method that considered the influence of rolling bearing clearance and flexible characteristics, using multibody dynamics theory and Hertz contact theory. They analyzed the motion error

of a crank-slider mechanism at different speeds. Lai et al. [21] examined the impact of radial clearance on a turbine expander rotor-bearing system, observing that a higher elastic support stiffness led to a narrower range of acceptable radial clearance. Smoli'k et al. [22] investigated the dynamic response of a turbocharger rotor while considering bearing radial clearance; their results demonstrated that certain clearance combinations effectively reduced the strength of subsynchronous rotor response. Li [23] proposed a new mathematical model and numerical method to analyze the contact behavior of rolling bearings. The results of contact stress and radial stiffness obtained from the traditional Hertz method and the new method are compared, showing that the new method yields more accurate results. Xu et al. [24] developed a new model for radial and axial clearance fit considering the clearance between the bearing outer ring and the bearing seat in machine tool spindle bearing systems. They analyzed the contact performance of deep groove ball bearings and the vibration characteristics of the system under support tilt errors. Chen et al. [25] solved the oil film pressure of sliding bearings using the finite difference method and over-relaxation iteration method. They studied the response of dynamic characteristic coefficients in rotor systems to different bearing clearances and found that adjusting the clearance effectively reduces unbalanced vibrations. Wei et al. [26] studied the influence of bearing clearance and width on bearing stiffness, damping, oil film thickness, and rotor instability. They found that reducing clearance and increasing width improves the stability of the rotor-bearing system. The above research does not consider the influence of the oil film clearance of sliding bearings and the supporting effect on the torsional vibration characteristics of the crankshaft system.

Several studies have considered the effects of clearance and flexibility on the behavior of mechanisms [27–31]. Bauchau et al. [32] proposed a comprehensive modeling method for joints with clearance in nonlinear flexible multibody systems. They considered the hinged clearance of a crank-slider mechanism and studied the dynamic response of clearance and lubrication in flexible multibody systems. The results showed that the flexibility of the structure significantly influenced the contact force, while lubrication had little effect. Khemili et al. [33] investigated the dynamic behavior of a planar flexible crank-slider mechanism with clearance. By considering the flexibility of the connecting rod, they were able to reduce impact forces, slider acceleration, and torque, and their results were validated through experiments. Xu et al. [34] presented a general method for dynamic modeling and analysis of planar multibody systems with deep groove ball bearings with clearance, emphasizing the significant influence of clearance on the dynamic performance of the mechanism. Zhao et al. [35] proposed a numerical method to model and predict wear in rotating clearance joints in flexible multibody systems by combining wear prediction with multibody dynamics. They compared wear prediction results for the clearance joint between rigid and flexible planar crank-slider mechanisms, showing a slight reduction in wear prediction after considering component flexibility. Ebrahimi et al. [36] used the Lankarani-Nikravesh contact force model to study the influence of joint stiffness on the instantaneous natural frequency and vibration mode of a flexible four-bar linkage with clearance. They found that joint stiffness considerably affected the instantaneous natural frequency and corresponding vibration mode of the flexible multibody system. Zheng et al. [37] considered the flexibility of the crank and connecting rod, compared and analyzed the dynamic response of a crank-slider mechanism in a high-speed press with clearance under both no-load and rigid-flexible conditions, and investigated the effects of clearance size, input crankshaft speed, and clearance number on the dynamic response of the mechanism. Dong et al. [38] studied the dynamic characteristics of flexible multilink mechanisms with mixed clearance under different working conditions. Wang et al. [39] developed the dynamic characteristics of the spherical clearance of the

parallel mechanism and the flexibility of the rod pair system. Tian et al. [40] used a numerical method to derive a general modeling and analysis method for flexible multibody systems with cylindrical clearances, but the analysis content is relatively conventional, and it is difficult to deeply reveal the influence of clearances on torsional vibration characteristics of crankshaft systems, nor has it carried out optimization research on the size of mixed clearances.

Furthermore, the rigid-flexible coupling method has been widely employed in studying the torsional vibrations of shafting systems [41–45]. Zhou et al. [46] established a rigid-flexible coupling multibody dynamics model of an engine crankshaft system using ADAMS software based on multibody dynamics theory. They then analyzed the angular vibration of the crankshaft to measure its dynamic characteristics. Wang et al. [47], considering the flexibility of the crankshaft, developed a rigid-flexible coupling multibody dynamics model of an engine crankshaft system. They solved for the torsional amplitude and resonance velocity of the shafting and verified the accuracy of the simulation results through torsional vibration tests. Qin et al. [48] investigated the dynamics of internal combustion engine crankshaft systems considering crankshaft flexibility. They analyzed the influence of the flexible crankshaft on bearing forces. Drab et al. [49] conducted a dynamic simulation analysis of an engine crankshaft characterized by a flexible body and explored the interaction forces between flexible bodies. Lv et al. [50] combined finite element analysis and multibody dynamics to analyze the rigid-flexible coupling of a crankshaft assembly, studying the load changes and dynamic characteristics of key components. Their results showed that flexible support can reduce the load on the crankshaft. Furthermore, Nowakowski et al. [51] emphasized that the elastic effect of the crankshaft cannot be ignored.

The above-mentioned research demonstrates that motion clearance and flexibility of mechanisms have a significant impact on motion accuracy and dynamic response. On the whole, most of the researches of existing scholars focus on the influence of the law of clearance on the dynamic response characteristics of flexible mechanisms, usually analyzing the dynamic characteristics change the law of the system under different working conditions or lubrication conditions and most of the researches stay in the analysis of the kinematic characteristics and load level of the mechanism, without carrying out the optimization design of clearance. More importantly, there are few reports on the influence of clearance on the torsional vibration of compressor flexible crankshaft systems, and there are few comprehensive analyses combining motion accuracy, force characteristics, torsional vibration characteristics, and vibration reduction optimization. In order to deeply and accurately reveal the effect of clearance and shafting flexibility on the torsional vibration of compressor crankshaft, this paper takes the crankshaft system of shale gas reciprocating compressor as the research object, aiming at the operation characteristics of compressor facing multiple Wells and variable loads. The study investigates the torsional vibration characteristics of a flexible compressor rotor system by considering mixed clearance, including crosshead pin clearance and sliding bearing clearance, and flexible characteristics of components in shale gas compressor crankshaft systems. The accuracy of the simulation model and results is verified through experiments. Based on this, an optimization of mixed clearance allocation is conducted to determine the minimum clearance configuration for torsional vibration, guiding accurate calculation of the torsional vibration response of crankshaft systems and improving the operational stability of compressors. The research process of this paper is shown in Fig. 2.
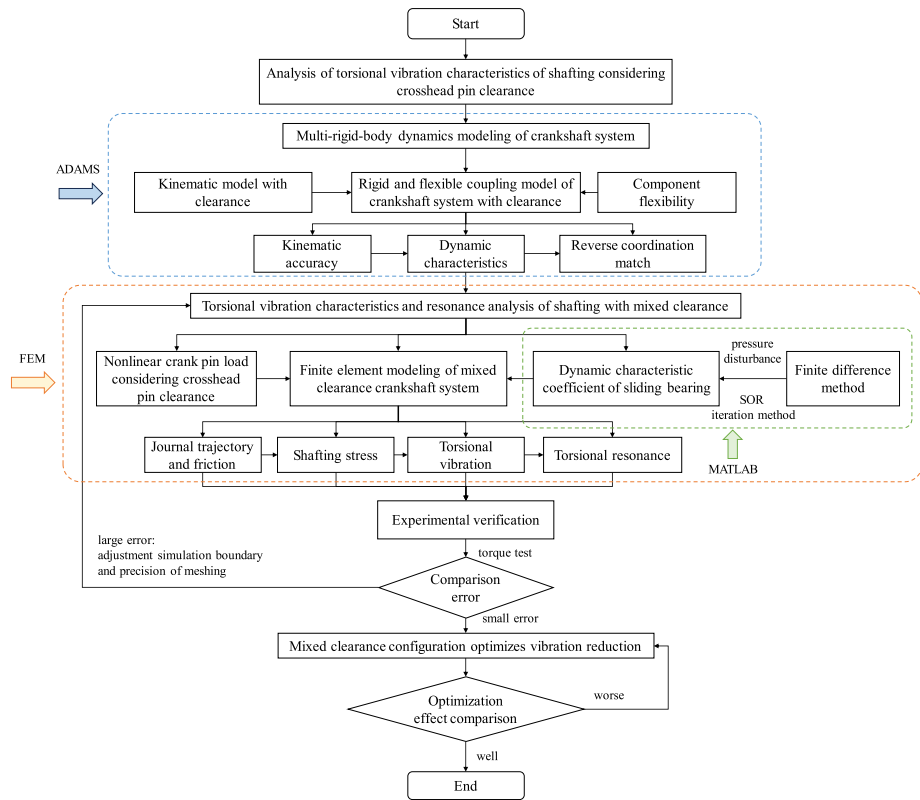
Fig. 2 Research content flow chart

2 Establishment of rigid-flexible coupling multibody dynamics model of compressor crankshaft system considering crosshead pin clearance

2.1 Collision force model of clearance motion pair

This section focuses on the clearance contact between the connecting rod bushing and the crosshead pin in the compressor crankshaft system. c is the radius difference. The vector diagram before and after the collision of the kinematic pair clearance is shown in Fig. 3. When the collision contact occurs, the collision insertion depth is h, Q is the collision contact point, the radius of the connecting rod bushing hole is r_i, and the radius of the pin shaft is r_j.
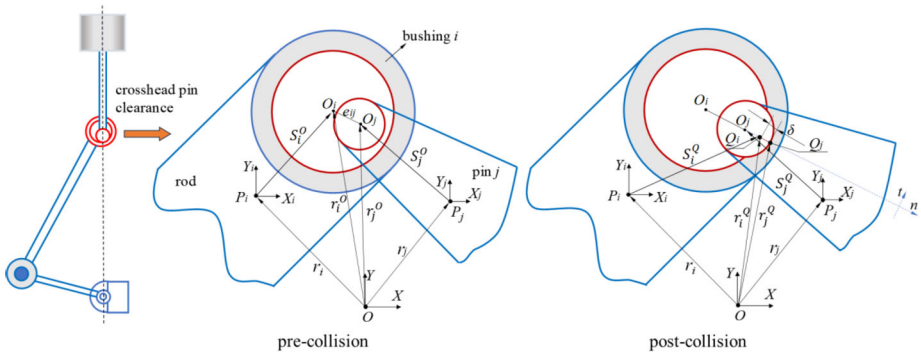
Fig. 3 Contact model of revolute clearance joint

Based on the Fig. 3, the vector relationship of the clearance model can be described as follows:

$$
\begin{cases}
h = r_j^Q - r_i^Q \\
e_{ij} = r_j^O - r_i^O \\
r_k^Q = r_k + A_k S_k + r_k n, \ (k = i, j) \\
\dot{r}_k^Q = \dot{r}_k + \dot{A}_k S_k + r_k \dot{n} \\
v = \left(\dot{r}_j^Q - \dot{r}_i^Q \right) + \left(\dot{A}_j S_j - \dot{A}_i S_i \right) + \left(R_j - R_i \right) \dot{n} \\
v_t = (\dot{r}_j^Q - \dot{r}_i^Q) t \\
v_n = (\dot{r}_j^Q - \dot{r}_i^Q) n
\end{cases}
\tag{1}
$$

where the e_{ij} is the center distance vector of the pin shaft and the bushing hole, which is normalized to obtain the unit vector n, S_k is the position vector of the axis in the dynamic coordinate system P_i and P_j, v is the relative collision speed between the bushing and the pin shaft, n is the unit normal vector, and is the position and velocity vector of the collision point in the inertial coordinate system O, respectively, A represents the transformation matrix of the dynamic coordinate system and the relative inertial coordinate system, and v_t and v_n denote the tangential and normal velocities of the contact surface.

The Lankarani-Nikravesh model and the hybrid model based on the improved elastic foundation contact model [11] are used to describe the contact force at the clearance:

$$
F_N = K_n h^n + Cv
\tag{2}
$$

The nonlinear contact stiffness coefficient K_n and damping coefficient C can be expressed as [52]:

$$
\begin{cases}
K_n = \frac{1}{8} \pi E^* \sqrt{\frac{2h(3c + 2h)^2}{(c + h)^3}} \\
E^* = \frac{E_j \left(1 - \mu_i^2 \right) + E_i \left(1 - \mu_j^2 \right)}{E_i E_j} \\
C = 0.75 K_n \left(1 - \varepsilon^2 \right) e^{2(1 - \varepsilon)} h^n / v_0
\end{cases}
\tag{3}
$$

where E_i, E_j, μ_i, μ_j are the elastic modulus and Poisson ratio of the bushing and the pin shaft, respectively, v_0 is the initial relative collision velocity, ε is the coefficient of restitution, and n is the force index of the metal surface.

Considering the relative sliding velocity of the contact between two objects along the tangential direction, the modified Coulomb friction model considering the dynamic friction coefficient is used to describe the friction F_f at the clearance:

$$F_f = -F_N \frac{v_t}{|v_t|} \mu_f(v_t) \tag{4}$$

The expression of the dynamic friction coefficient [10] is as follows:

$$\mu_f(v_t) = \begin{cases} -\mu_d sign(v_t) & |v_t| \leq v_d \\ -\{\mu_d + (\mu_s - \mu_d)\} \left(\frac{|v_t|-v_s}{v_d-v_s}\right)^2 \left[3 - 2\left(\frac{|v_t|-v_s}{v_d-v_s}\right)\right] sign(v_t) & v_s < |v_t| \leq v_d \\ \mu_s - 2\mu_s \left(\frac{v_t+v_s}{2v_s}\right)^2 \left(3 - \frac{v_t+v_s}{v_s}\right) & |v_t| < v_s \end{cases} \tag{5}$$

where v_1 and v_0 are the upper and lower limits of the relative tangential velocity between the bushing and the pin shaft, μ_d is the dynamic friction coefficient, μ_s is the static friction coefficient, v_s is the critical velocity of static friction, and v_d is the maximum dynamic friction critical velocity.

2.2 Establishment of rigid-flexible coupling dynamic model of shafting considering clearance

Multiple studies have shown that multi-flexible body dynamics can provide a more comprehensive understanding of the dynamic characteristics of mechanical systems [53, 54]. The motion of a flexible body is divided into motion relative to a moving reference system caused by deformation, and the flexibility of the structure is represented through superposition. The position of the flexible body node can be composed of three vectors:

$$\vec{r} = \vec{x} + \vec{s} + \vec{u} \tag{6}$$

where $\vec{x}$ is the displacement of the body reference system relative to the inertial reference system, $\vec{s}$ is the displacement of the node relative to the body reference system before deformation, and $\vec{u}$ is the displacement of the post-deformation node relative to the pre-deformation.

The position of the crankshaft system is represented by the Cartesian coordinate $l = (x, y, z)$, and the Euler angle $\psi = (\varphi, \theta, \varphi)$ reflecting the orientation of the rigid crankshaft system. The modal coordinates are expressed by $q = (q_1, q_2, \ldots, q_n)^T$ (n is the number of modal coordinates). The generalized coordinates of the flexible body are obtained by combining the rigid body and flexible body coordinates:

$$\boldsymbol{\xi} = \left[\mathbf{l}, \boldsymbol{\psi}, \mathbf{q}_{j, j=1,\ldots,n}\right]^T \tag{7}$$

For the variable topology multibody system with discontinuous contact collision, the contact state is constantly changing. The step function $\mu(h)$ is introduced, and the constraint force F_C can be expressed as follows:

$$\begin{cases} F_C = (F_N + F_f)u(h) \\ u(h) = \begin{cases} 0, & h \leq 0 \\ 1, & h > 0 \end{cases} \end{cases} \tag{8}$$
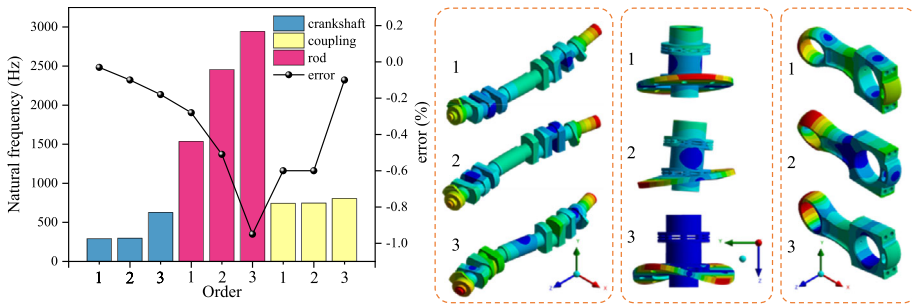
Fig. 4 Modal information of condensed model

The collision contact force F_c is introduced into the dynamic model as a generalized external force, and the differential equation of multi-flexible body dynamic motion of crankshaft system with joint clearance based on the Lagrange equation is obtained [55, 56]:

$$\begin{cases} \mathbf{M}\ddot{\xi} + \mathbf{C}\dot{\xi} + \mathbf{K}\xi + \boldsymbol{\varphi}_\xi^T \lambda = \mathbf{Q} + \boldsymbol{\alpha}_\xi \mathbf{F}_C \\ \boldsymbol{\varphi}(\xi, t) = 0 \end{cases} \tag{9}$$

where $\xi, \dot{\xi}, \ddot{\xi}$ are the generalized coordinate vector corresponding to the finite element node of the flexible crankshaft system and its first and second derivatives with respect to time, $\mathbf{M}$, $\mathbf{K}$, $\mathbf{C}$, and $\mathbf{Q}$ are the mass matrix, stiffness matrix, damping matrix, and generalized force matrix without collision force of flexible crankshaft system, respectively, $\boldsymbol{\varphi}_\xi$ is the Jacobian matrix of the constraint equation of the crankshaft system, λ is the Lagrange multiplier array, $\boldsymbol{\varphi}(\xi, t)$ is a non-ideal hinge constraint equation, $\boldsymbol{\alpha}_\xi$ is the coordinate transformation matrix from the global coordinate system to the generalized coordinate system, and $\boldsymbol{Fc}$ is the generalized contact force of Cartesian generalized coordinate ξ.

3 Torsional vibration characteristics analysis of compressor crankshaft system considering crosshead pin clearance

3.1 Establishment of rigid-flexible coupling dynamics simulation model of shafting

In the crankshaft system of reciprocating compressor, the coupling, crankshaft, and connecting rod are crucial power transmission components responsible for bearing force and torque. Their flexible characteristics greatly influence the torsional vibration response of the crankshaft system. In this study, these components are treated as flexible bodies.

The realization of the flexible body is to reduce the finite element model by the modal reduction technique (Craig-Bampton component integrated modal method) [57, 58]. The modal information of the first three non-zero condensed models is compared to the finite element model, as shown in Fig. 4. The modal shapes of the two are basically the same, and the natural frequency error is small. The condensed model slightly underestimates the natural frequency, with an error within 1%. This indicates that the model retains accurate information.

To establish a rigid-flexible coupling dynamics simulation model, the flexible bodies are imported into ADAMS, and the connection relationships between components are accurately defined. The motor rotor speed is added, and material properties are applied to each

component. The gas force of the double-acting piston is calculated based on the gas pressure data on both sides of the piston, as described by formula (10). The gas force spline data is then added to the piston using a cubic spline fitting function, CUBSPL, to simulate the gas force:

$$F_g = P_{CE} A_{CE} - P_{HE} A_{HE} \tag{10}$$

The hybrid model of the clearance vector model, clearance contact collision force, and modified friction model are embedded in the IMPACT function within the ADAMS software. The collision force [31, 37] is as follows:

$$F_N = K_n h^n + C(h) v \tag{11}$$

$$C(h) = \text{step}(h, h_0, C_0, h_{\max}, C_{\max})$$
$$= \begin{cases} C_{\max} & h \geq h_{\max} \\ C_{\max} \left(\frac{h-h_0}{h_{\max}-h_0} \right)^2 \left(3 - 2 \left(\frac{h-h_0}{h_{\max}-h_0} \right) \right) & h_0 < h < h_{\max} \\ C_0 & h \leq h_0 \end{cases} \tag{12}$$

where $C(h)$ is the instantaneous normal damping coefficient, a third-order function of the intrusion value h.

The parameters of the crankshaft system are shown in Table 1.

The collision force is specifically applied between the connecting rod bushing and the crosshead pin shaft, while the other kinematic pairs are treated as ideal connections. Gravity is added, and the rigid-flexible coupling dynamic simulation model of the crankshaft system with clearance is established, as shown in Fig. 5.

3.2 Analysis of dynamic characteristics of crankshaft system

In this section, the rigid-flexible coupling dynamic model of the crankshaft system with clearance is simulated and analyzed. After ignoring the initial iteration error, the dynamic response of the shafting is analyzed during the second period. The motion characteristics and motion error of a column of pistons in the compressor are selected and analyzed to evaluate the influence of clearance on the motion accuracy of the shafting. The variation of the transmission torque on both sides of the coupling is also solved and analyzed to judge the influence of clearance on the stability of power transmission in shafting. Finally, the influence of clearance on the torsional coordination of the shaft section is analyzed using the phase trajectory of the shaft section.

3.2.1 Kinematic accuracy analysis of crankshaft system

The displacement, velocity, and acceleration changes of a series of pistons in the compressor, as well as their errors relative to ideal motion, are selected and analyzed, as shown in Fig. 6.

Figure 6 depicts the motion characteristic curve of the piston and the error between the motion with clearance and without clearance in the rigid-flexible coupling dynamic model of the crankshaft system in a cycle. Initially, the piston is in the middle of the compression cylinder. Analysis of the piston displacement curve reveals a smooth, sinusoidal-like motion with no significant oscillations, conforming to the expected behavior of a sine function. The overall fluctuation of displacement error is small and within the allowable clearance of ± 0.1 mm. The maximum displacement error occurs at a crankshaft angle of approximately 552°, reaching -0.098 mm. In Fig. 6(b), the speed varies within the range

Table 1 Simulation parameters of the compressor crankshaft system with clearance

Parameters			Values
Working parameter		Driving speed(RPM)	1486
		Piston stroke(mm)	88.9
		Intake/Exhaust pressure(MPa)	0.77/4.34
		Shaft power(kW)	485
Collision parameter		Static friction coefficient	0.08
		Dynamic friction coefficient	0.05
		Force exponent	1.5
		Permit penetration depth	1.0e-6
		Material recovery coefficient	0.9
Physical parameters of key components	Crankshaft,Rod	Modulus of elasticity(GPa)	212
		Poisson's ratio	0.28
		Density(kg/m^3)	7850
	Coupling	Modulus of elasticity(GPa)	211
		Poisson's ratio	0.28
		Density(kg/m^3)	7860
		Total moment of inertia(kg m^2)	2.8589
		Torsional Stiffness(Nm/rad)	9.4116e6
	Rod bushing	Internal diameter(mm)	65.0
		Modulus of elasticity(GPa)	95
		Poisson's ratio	0.32
		Density(kg/m^3)	8760
	Crosshead pin	External diameter(mm)	64.8
		Modulus of elasticity(GPa)	207
		Poisson's ratio	0.254
		Density(kg/m^3)	7870
	Motor shaft	Mass(kg)	2258.2
		Rotor core inertia(kg m^2)	15.96
		Torsional Stiffness(Nm/rad)	3.1277e7

of $-7.07\sim7.06$ m/s. Two clear error peaks are observed in the speed error curve, corresponding to crankshaft angles of 419° and 613°, with values of -0.21 m/s and 0.29 m/s, respectively. These peaks may be attributed to contact collisions at the clearance, but due to component constraints, the speed variation remains relatively stable with small errors. The acceleration range in the Fig. 6(c) is -1410.84$\sim$1312.31 m/s^2. The curve exhibits noticeable nonlinear oscillations, and the error curve also displays two peak points of 747.8 m/s^2 and -1693.14 m/s^2, respectively. The maximum error in piston acceleration reaches 400.1%. These results suggest that clearance significantly influences piston dynamic characteristics in the order of acceleration＞velocity＞displacement.

Compared to the motion curve of the crankshaft system without clearance, the crankshaft system with clearance exhibits nonlinear vibration characteristics. However, the motion characteristics of the system with clearance still align with the theoretical research within the allowable error range.
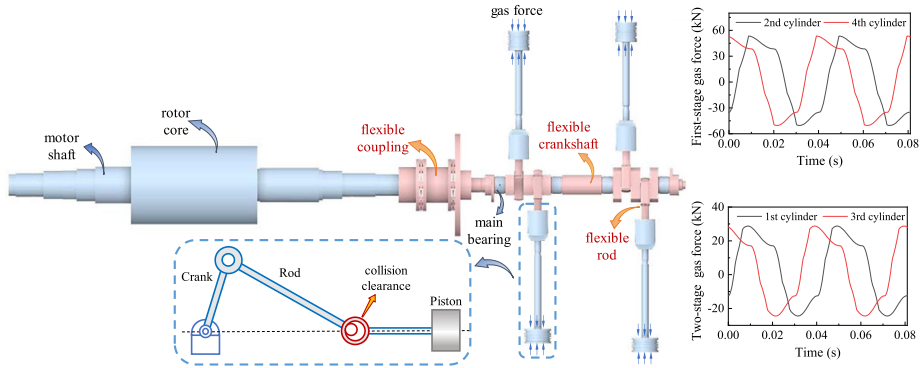
Fig. 5 Rigid-flexible coupling model of crankshaft system with clearance

(a) Displacement of piston

(b) Velocity of piston

(c) Acceleration of piston
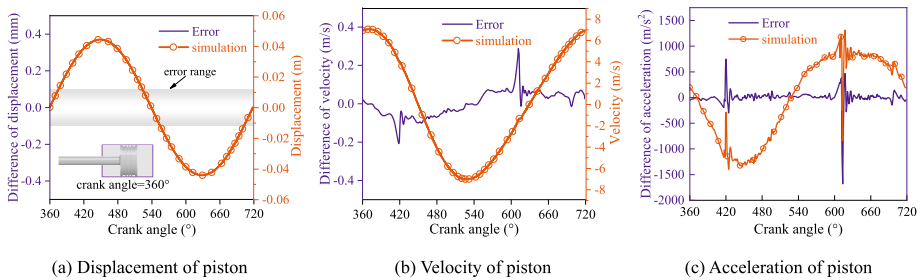
Fig. 6 The dynamic characteristic and error of piston

### 3.2.2 Power transmission matching of crankshaft system

The torque transmission on both sides of the elastic coupling shows a lag phenomenon, which can potentially lead to instability in the power output of the crankshaft system. This is one of the main reasons for the torsional vibration of the shafting. Therefore, the dynamic torque on both sides of the coupling, namely the motor side and the crankshaft side, is calculated, and their difference is analyzed.

Figure 7(a) illustrates that the changing trend of the dynamic torque at the coupling crankshaft end is nearly identical with or without considering the clearance. The maximum torque occurs at a crank angle of about 460°. However, when considering the clearance, the torque is generally larger, with a maximum torque of 3579.03 N m, which indicates an increase of 5.88%. From Fig. 7(b), it is observed that the torque amplitude appears at the fundamental frequency of the motor ($f_0 = 24.77$ Hz) and its multiples, with the most significant amplitude occurring at the fundamental frequency and its fourth harmonic. Taking clearance into account, the amplitude corresponding to the third and fourth harmonics decreases while other frequency components increase. This suggests that the risk of torsional vibration in the shafting increases when considering clearance.

From Fig. 7(c), it is evident that the torque at the motor end is greater than that at the crankshaft end. At this moment, the torque at the crankshaft end exhibits a lag state, with the proportion of integral area above T = 0 N m representing the lag rate. The calculation indicates that the lag rate of the torque at the crankshaft end is 58.4% and 54.5%, respectively.
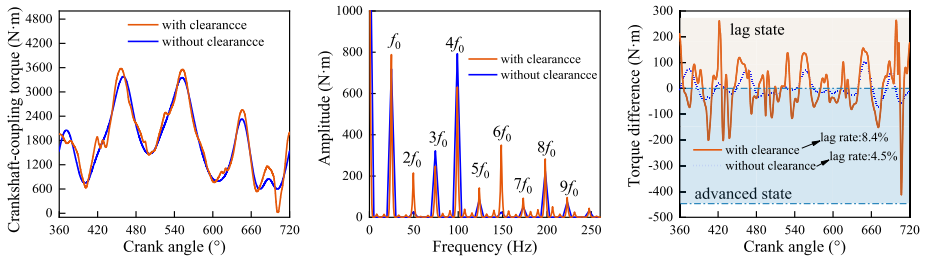
Fig. 7 Curve of dynamic torque in crankshaft system. (a) The time domain variation curve of the dynamic torque of the coupling-crankshaft end under the condition of considering the clearance and not considering the clearance. (b) The frequency domain variation of the dynamic torque curve of the coupling-crankshaft end. (c) The time domain variation curve of the difference between the dynamic torque of the coupling-motor end and the coupling-crankshaft end
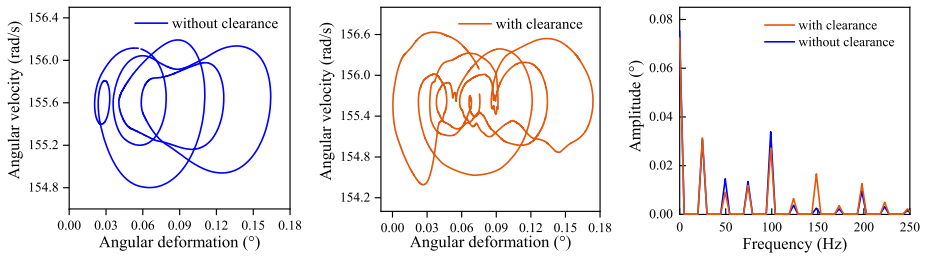
Fig. 8 The phase trajectory of the coupling-crankshaft connection section. (a) does not consider the phase trajectory of the shaft section under the clearance. (b) considers the phase trajectory of the shaft section under the clearance. (c) angular displacement spectrum

This indicates that the dynamic torque at the crankshaft end lags behind the one at the motor end as a whole. Furthermore, the lag rate at the crankshaft end is greater when considering the clearance, indicating that clearance reduces the power transmission performance of the crankshaft system.

3.2.3 Torsion coordination of crankshaft section

In Fig. 8(a), when clearance is not considered, the phase trajectory of the shaft section consists of multiple nonoverlapping elliptical orbits. When clearance is not included, the head and the tail of the phase trajectory are connected, forming a complete loop. This represents an ideal periodic motion, confirming the stability of the shaft system. The angular displacement amplitude of the shaft section is 0.164°, and the fluctuation range of angular velocity in the shaft system is observed to be between 154.80 and 156.19 rad/s. According to the mechanical design manual, the operating non-uniformity coefficient ζ, calculated using formula (13), is 0.0089, which meets the required limit of 0.0125 for electric drive reciprocating compressors, meeting the operational requirements.

$$\zeta = \frac{\omega_{\max} - \omega_{\min}}{\omega_{\mathrm{m}}} \tag{13}$$

In Fig. 8(b), after considering the clearance, the phase trajectory becomes significantly staggered, with the head and tail of the trajectory lines no longer connecting. The crankshaft
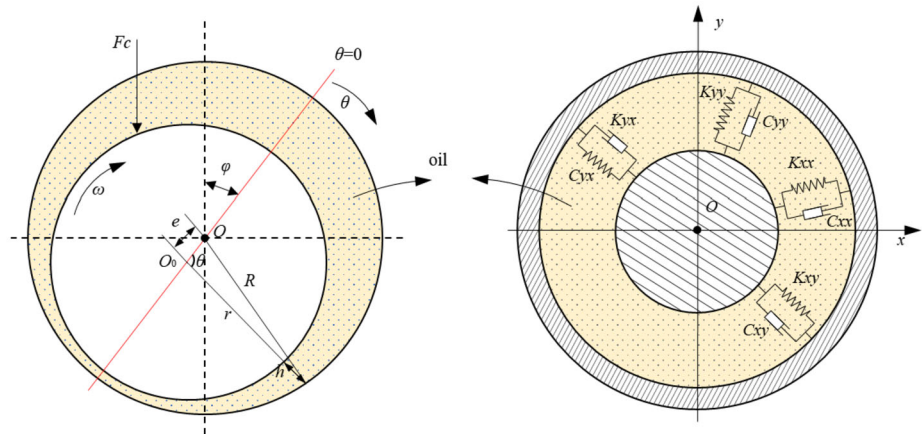
Fig. 9 Dynamic model of sliding bearing

system undergoes quasi-periodic motion. The fluctuation range of the angular velocity in the shafting shifts from 154.39 to 156.63 rad/s, and the operating non-uniformity coefficient reaches 0.0144, exceeding the requirements for compressor operation. Additionally, the angular displacement amplitude reaches 0.174°, which is 6.10% higher compared to not considering clearance.

In Fig. 8(c), after considering clearance, the angular displacement amplitude decreases for the 2nd, 3rd, and 4th harmonics, while the proportion of the remaining frequency doubling components increases, making the composition more complex. The main frequency is reduced from four times to one time, which amplifies the torsional amplitude of the shafting. Generally, clearance reduces the dynamic performance and deteriorates the torsional coordination of the compressor's shafting. However, it is important to note that the results may be overestimated due to the lack of consideration for the oil film support effect of the sliding bearing.

4 Torsional vibration characteristics analysis of compressor crankshaft system considering mixed clearance

References [29, 34, 35, 59, 60] have highlighted the significant influence of clearance and part flexibility on the force and motion accuracy of a motion system. Building upon the previous analysis, this study investigates the effects of mixed clearance on the torsional vibration characteristics of the crankshaft system by considering both the crosshead pin clearance and the sliding bearing clearance.

4.1 Dynamic model of sliding bearing clearance

The dynamic model of a radial sliding bearing, taking into account the oil film clearance between the crankshaft and the bearing, is established as shown in Fig. 9. The bearing hole diameter is denoted as R, and the journal radius as r. Under the external load F_c, there exists an eccentricity e between the journal center and the bearing center, along with an offset angle φ. The oil film thickness is represented by h.
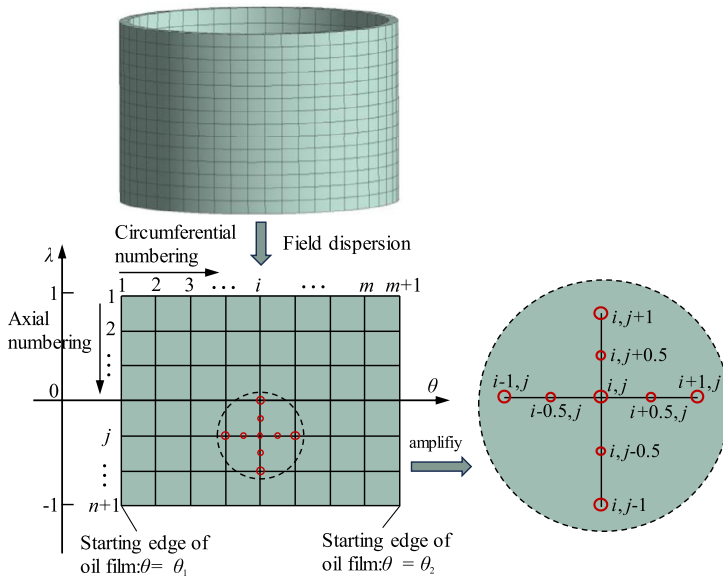
Fig. 10 Oil film field dispersion on bearing surface

By employing the cosine theorem and geometric relationships, it can be determined that the nominal oil film thickness of the bearing bush at any position [61] is given by:

$$\delta = c_0(1 + \varepsilon \cos\theta) \tag{14}$$

Here, the eccentricity is defined as $\varepsilon = e/c_0$, with the radius clearance represented by $c_0 = R - r$. Under certain assumptions, the dimensionless form of the static Reynolds equation for the radial sliding bearing [62] is obtained as follows:

$$\frac{\partial}{\partial\theta}\left[H^3\frac{\partial P}{\partial\theta}\right] + \left(\frac{D}{L}\right)^2\frac{\partial}{\partial\lambda}\left[H^3\frac{\partial P}{\partial\lambda}\right] = 3\frac{\partial H}{\partial\theta} \tag{15}$$

The above formula is a second-order nonlinear partial differential equation, where $\delta = c_0 H$, D/L is the ratio of bearing width to diameter. The finite difference method is utilized to discretize the field of the bearing bush in order to ensure accuracy and efficiency, as shown in Fig. 10.

In Fig. 10, the pressure at node (i, j) is represented by $P_{i,j}$. The partial derivatives of node pressure to angle and pressure to axial position in equation (15) can be differentially transformed by using the half-step difference method. The second-order partial derivations can be nested by the same method and can finally be converted into the following difference formula:

$$\begin{cases} \left(\frac{\partial P}{\partial\theta}\right)_{i,j} \approx \frac{P_{i+0.5,j}-P_{i-0.5,j}}{\Delta\theta}, \left(\frac{\partial P}{\partial\lambda}\right)_{i,j} \approx \frac{P_{i,j+0.5}-P_{i,j-0.5}}{\Delta\lambda}, \left(\frac{\partial H}{\partial\theta}\right)_{i,j} \approx \frac{H_{i+0.5,j}-H_{i-0.5,j}}{\Delta\theta} \\ \frac{H^3_{i+0.5,j}(P_{i+1,j}-P_{i,j})-H^3_{i-0.5,j}(P_{i,j}-P_{i,-1j})}{(\Delta\theta)^2} + \\ \left(\frac{d}{L}\right)^2\frac{H^3_{i,j+0.5}(P_{i,j+1}-P_{i,j})-H^3_{i,j-0.5}(P_{i,j}-P_{i,j-1})}{(\Delta\lambda)^2} = \frac{3(H_{i+0.5,j}-H_{i-0.5,j})}{\Delta\theta} \end{cases} \tag{16}$$

where $P_{i,j}$ is the oil film pressure on the node (i, j), and $H_{i,j}$ is the thickness of the oil film on the node (i, j).

Equation (16) can be simplified into the following form:

$$
\begin{cases}
P_{i,j} = \frac{A_{i,j} P_{i+1,j} + B_{i,j} P_{i-1,j} + C_{i,j} P_{i,j+1} + D_{i,j} P_{i,j-1} - F_{i,j}}{E_{i,j}} \\
A_{i,j} = \frac{H_{i+0.5,j}^3}{(\Delta\theta)^2}, \, B_{i,j} = \frac{H_{i-0.5,j}^3}{(\Delta\theta)^2}, \, C_{i,j} = \left(\frac{d}{L}\right)^2 \frac{H_{i,j+0.5}^3}{(\Delta\lambda)^2}, \, D_{i,j} = \left(\frac{d}{L}\right)^2 \frac{H_{i,j-0.5}^3}{(\Delta\lambda)^2} \\
E_{i,j} = A_{i,j} + B_{i,j} + C_{i,j} + D_{i,j}, \, F_{i,j} = \frac{3\left(H_{i+0.5,j}^3 - H_{i-0.5,j}^3\right)}{\Delta\theta}
\end{cases}
\quad (17)
$$

When equation (16) includes all nodes in the bearing bush grid, a set of linear nonhomogeneous algebraic equations containing $P_{i,j}$ values of $(m\text{-}1)(n\text{-}1)$ inner nodes can be formed. The number of circumferential grids is set as $m = 60$, and the axial grid as $n = 40$. The pressure values of nodes near nodes (i, j) can be solved by the overrelaxation iterative method to obtain the oil film pressure distribution of the bearing bush under the static Reynolds equation (15). Reynolds boundary conditions and iterative convergence accuracy are:

$$
\begin{cases}
p(\theta_1, \frac{L}{2}) = p(\theta_2, -\frac{L}{2}) = 0 \\
\frac{\partial p}{\partial \theta}\big|_{\theta=\theta_1} = \frac{\partial p}{\partial \theta}\big|_{\theta=\theta_2} = 0 \\
\sum_{i=2}^{m} \sum_{j=2}^{n} \left| \frac{P_{i,j} - P_{i,j}'}{P_{i,j}} \right| \leq \varepsilon_0
\end{cases}
\quad (18)
$$

When the crankshaft system is running smoothly, the crankshaft journal will be subjected to a small displacement or velocity disturbance in the static equilibrium position. At this time, the nonlinear relationship between the oil film reaction of the bearing bush and the disturbance is linearized, and the stiffness and damping are related to each other through the disturbance displacement and velocity.

Considering the disturbance of small displacement Δx, Δy, and velocity x', y', the dimensionless form of unsteady motion Reynolds equation becomes:

$$
\frac{\partial}{\partial \theta}\left[\frac{H^3}{\eta} \frac{\partial P}{\partial \theta}\right] + \left(\frac{D}{L}\right)^2 \frac{\partial}{\partial \lambda}\left[\frac{H^3}{\eta} \frac{\partial P}{\partial \lambda}\right] = \frac{3\partial H}{\partial \theta} + 6\left(y' \cos\theta + x' \sin\theta\right)
\quad (19)
$$

$$
\begin{cases}
H = H_0 + \Delta x \sin\theta + \Delta y \cos\theta \\
P = P_0 + P_x \Delta x + P_y \Delta y + P_{x'} x' + P_{y'} y'
\end{cases}
\quad (20)
$$

Where x' and y' are the extrusion velocity of the journal center in the x and y directions.

By combining formulas (17) and (18), the differential equation of the disturbance pressure is obtained by ignoring small quantities of higher order:

$$
\left[\frac{\partial}{\partial \theta}\left(H_0^3 \frac{\partial}{\partial \theta}\right) + \left(\frac{d}{L}\right)^2 \frac{\partial}{\partial \lambda}\left(H_0^3 \frac{\partial}{\partial \lambda}\right)\right]
\begin{Bmatrix} P_x \\ P_y \\ P_{x'} \\ P_{yy} \end{Bmatrix}
$$
$$
=
\begin{cases}
3\cos\theta - 9\frac{\sin\theta}{H_0} \frac{\partial H_0}{\partial \theta} - 3H_0^3 \frac{\partial}{\partial \theta}\left(\frac{\sin\theta}{H_0}\right) \frac{\partial P_0}{\partial \theta} \\
-3\sin\theta - 9\frac{\cos\theta}{H_0} \frac{\partial H}{\partial \theta} - 3H_0^3 \frac{\partial}{\partial \theta}\left(\frac{\cos\theta}{H_0}\right) \frac{\partial P_0}{\partial \theta} \\
6\sin\theta \\
6\cos\theta
\end{cases}
\quad (21)
$$

Table 2 Sliding bearing parameters

Structural parameter	Value	Dimensionless stiffness coefficient K_{ij}	Value	Dimensionless damping coefficient C_{ij}	Value
Bearing width L/mm	48.2	K_{xx}	1.213	C_{xx}	2.469
Bearing inner diameter D/mm	89	K_{xy}	−2.700	C_{xy}	2.138
Eccentricity ε	0.6	K_{yx}	1.090	C_{yx}	2.257
Clearance c/mm	0.10	K_{yy}	3.556	C_{yy}	6.297
Viscosity η/(pa s)	0.018				
Rotor speed N/(r/min)	1486				

where P represents the oil film pressure, η is the oil film viscosity, θ is the coordinate of the journal circumference angle, z is the coordinate of the axial direction, and ω is the angular velocity of the journal.

Equation (21) is also a second-order partial differential equation; the above difference method and overrelaxation iterative method are used to discreetly solve the distribution pressure of P_x, P_y, $P_{x'}$ and $P_{y'}$, and then the dimensionless dynamic characteristic coefficient of the main bearing can be solved by Simpson integral in the oil film interval:

$$
\left.\begin{array}{l} K_{xx} \\ K_{yx} \end{array}\right\} = \int_{-1}^{1}\int_{0}^{2\pi} -P_x \left\{\begin{array}{l} \sin\theta \\ \cos\theta \end{array}\right. d\theta d\lambda, \quad \left.\begin{array}{l} K_{xy} \\ K_{yy} \end{array}\right\} = \int_{-1}^{1}\int_{0}^{2\pi} -P_y \left\{\begin{array}{l} \sin\theta \\ \cos\theta \end{array}\right. d\theta d\lambda
$$
$$
\left.\begin{array}{l} C_{xx} \\ C_{yx} \end{array}\right\} = \int_{-1}^{1}\int_{0}^{2\pi} -P_{x'} \left\{\begin{array}{l} \sin\theta \\ \cos\theta \end{array}\right. d\theta d\lambda, \quad \left.\begin{array}{l} C_{xy} \\ C_{yy} \end{array}\right\} = \int_{-1}^{1}\int_{0}^{2\pi} -P_{y'} \left\{\begin{array}{l} \sin\theta \\ \cos\theta \end{array}\right. d\theta d\lambda \tag{22}
$$

4.2 Establishment of finite element model of crankshaft system considering mixed clearance

The oil film stiffness and damping of sliding bearings have a significant impact on the stability of the crankshaft system. The dynamic characteristic coefficient of the bearing plays a crucial role in accurately analyzing the torsional vibration response of the crankshaft system. By combining the sliding bearing parameters with Eqs. (15–22), the finite difference method and the over-relaxation iteration method are employed to solve the bearing oil film pressure using MATLAB. Subsequently, the pressure perturbation method is utilized to solve the dynamic characteristic coefficient of the sliding bearing. The bearing parameters and dynamic characteristic coefficients are listed in Table 2.

To ensure simulation efficiency, reciprocating parts such as the piston, piston rod, crosshead, and small end of the connecting rod are simplified by equivalence. Additionally, installation parts on the motor rotor, such as the balance ring, wind ring, inner fan, and outer fan, also affect the torsional characteristics of the crankshaft system. Equivalent mass and equivalent rotational inertia are applied to the inertia node of the crank pin. The specific equivalent parameters are presented in Table 3.

The impact contact force, considering the crosshead pin clearance, is applied to the equivalent simplified crankshaft system in Ansys software. The oil film stiffness and damping act on the position of the main bearing to complete the bearing support constraint. This process builds a finite element simulation model considering the mixing clearance, as shown in Fig. 11.

Table 3 Equivalent information for the rest of the crankshaft system

Equivalent parts		Equivalent mass/kg	Equivalent motion inertia/(kg m^2)
Rotating parts	Balance ring	9	0.24
	Windshield ring	14.9	0.4
	External fan	23	0.7
	Inner fan	28.2	1.1
	rod in big-end	5.77	0.0114
Reciprocation parts	rod in small-end	2.89	0.0283
	Piston assembly	15.92	
	Crosshead	7.33	
	Crosshead pin	2.45	
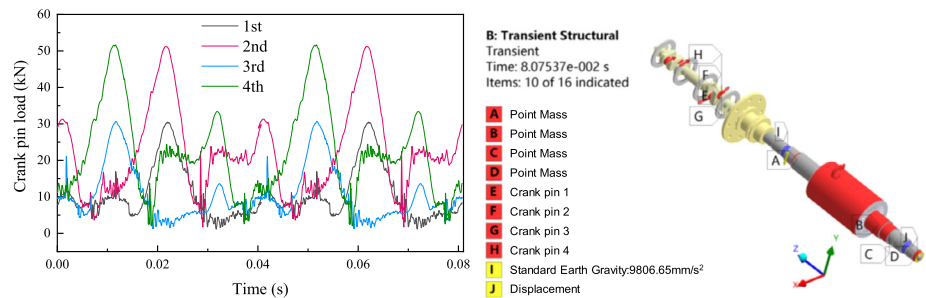
Fig. 11 Finite element model of crankshaft system with mixed clearance

4.3 Analysis of forced vibration response of crankshaft system

The dynamic characteristics of the crosshead pin clearance (CPC), the sliding bearing clearance (SBC), and the mixed clearance (MC) are solved, and the influence of different clearances on the torsional vibration of the shafting is compared and analyzed.

4.3.1 Dynamic characteristics analysis of crankshaft main journal

When considering the mixed clearance, due to the clearance between the main journal and the bearing, the running trajectories of the four crankshaft main journals can be determined, and the rub-impact between the crankshaft and the bearing bush is analyzed based on the limit positions of the trajectory curve, enabling the assessment of the stability of the shafting movement. The calculation results are shown in Fig. 12.

The X direction corresponds to the compression movement of the piston and experiences the maximum force. Therefore, the displacement in the X direction is longer compared to the Y direction, where gravity acts, and the force is smaller. As a result, each column of the main journal has a shorter displacement in the Y direction. The trajectory of each column of the journal is not perfectly circular, but the fourth column tends to have a circular trajectory, indicating a higher probability of contact with the bearing. Due to the flexibility and deformation of the parts, the X-direction displacement of the second, third, and fourth rows of the journal exceeds the maximum specified clearance value of 0.2 mm. The X direction
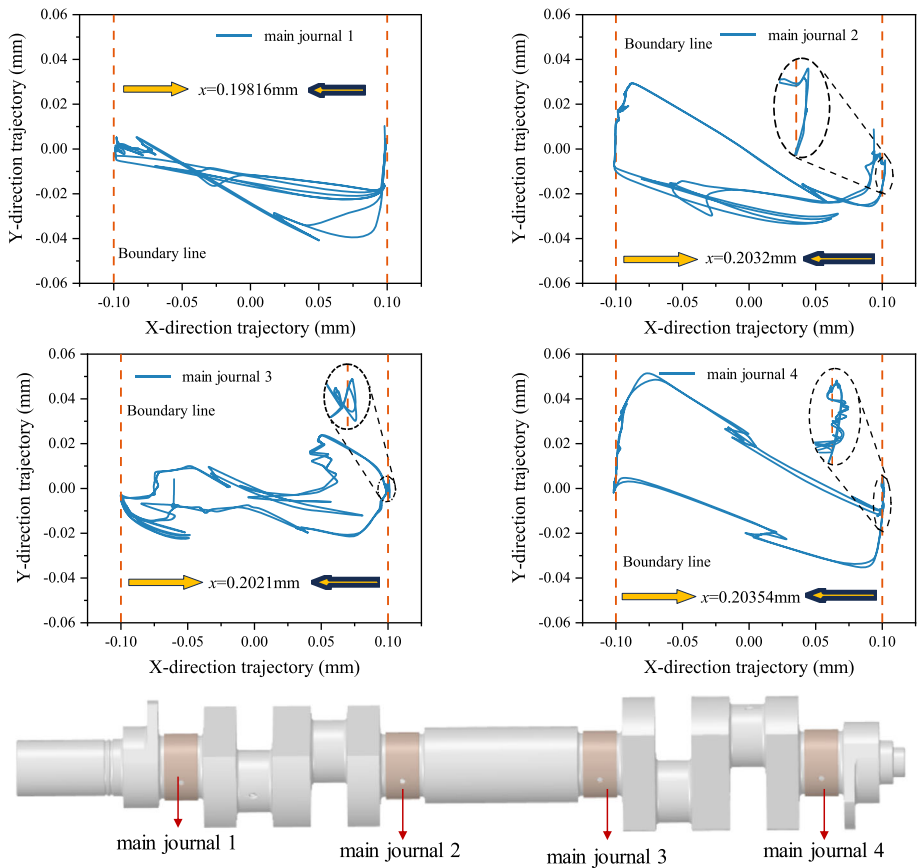
Fig. 12 Trajectory of the journal in the main bearing

displacement of the fourth row is the largest at 0.20354 mm, leading to rubbing between the shaft segment and the bearing, as shown in Fig. 13.

In Fig. 13, the analysis reveals that the SBC (Sliding Bearing Clearance) curve is smoother than the MC (Mixed Clearance) curve. The MC curve contains the collision clearance at the crosshead pin, exhibiting more pronounced nonlinear characteristics. However, the general trend of the two curves is similar. The maximum rubbing depth for MC and SBC is observed at the fourth row of the spindle neck, measuring 7.7μm and 5.6μm, respectively. The rubbing area for MC is concentrated on the right side of the bearing bush, indicating a more pronounced stress concentration phenomenon. On the other hand, the rubbing area for SBC extends to the left side of the bearing bush, resulting in a more uniform stress distribution and improved bearing capacity.

4.3.2 Crankshaft dynamic stress analysis

The dynamic stress analysis of the crankshaft in Fig. 14 shows that the stress curve for CPC fluctuates significantly. The maximum stress moment occurs at 0.069 s and is located at the second row of the spindle neck with a magnitude of 216.26 MPa, exhibiting obvious stress
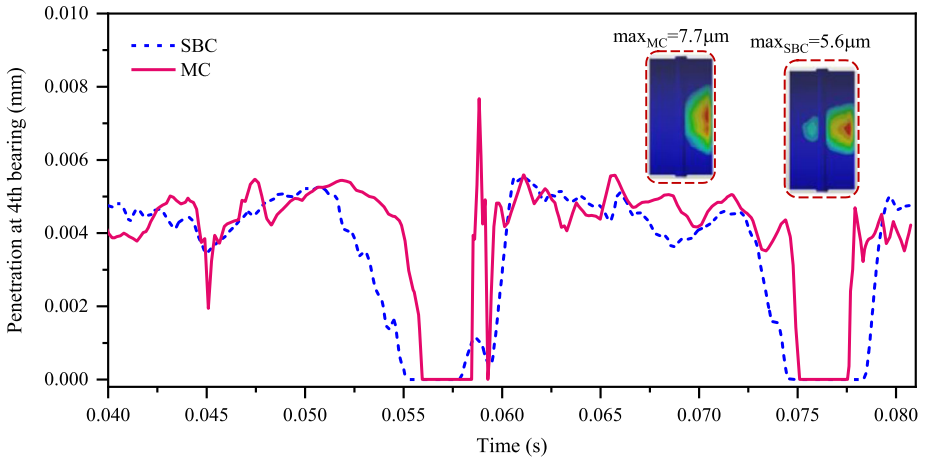
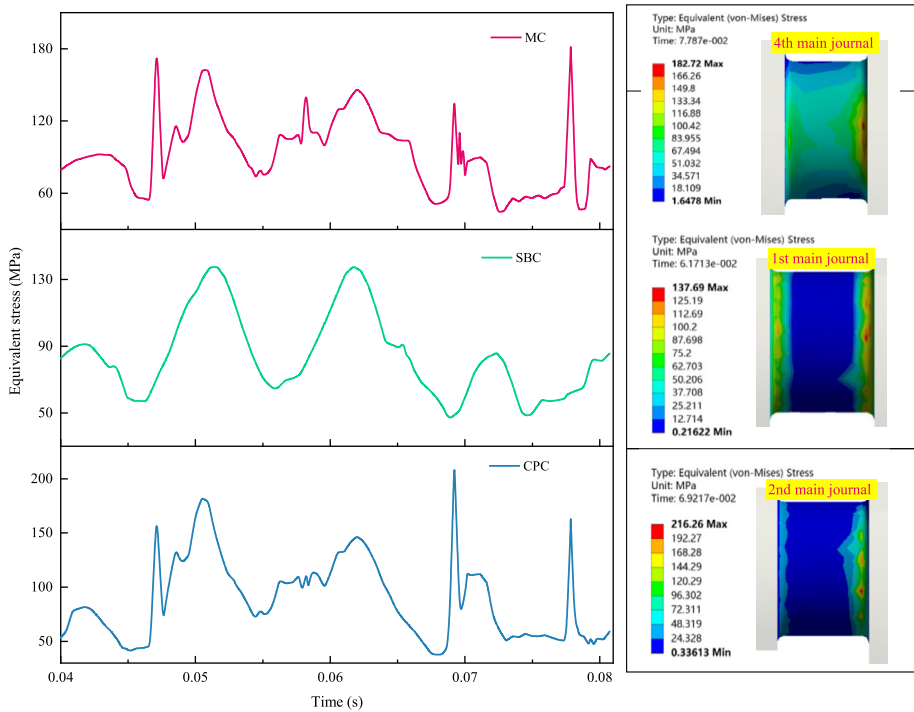**Fig. 13** The change of the rub-impact amount of the fourth bearing bush

Fig. 14 Crankshaft dynamic stress distribution

concentration. In contrast, the stress curve for SBC is relatively smooth without violent fluctuations. The maximum stress moment occurs at 0.062 s, measuring 137.69 MPa, which is 36.33% lower than that of CPC. The stress distribution for SBC is relatively uniform, with the maximum stress located at the rounded corners on both sides of the first row of
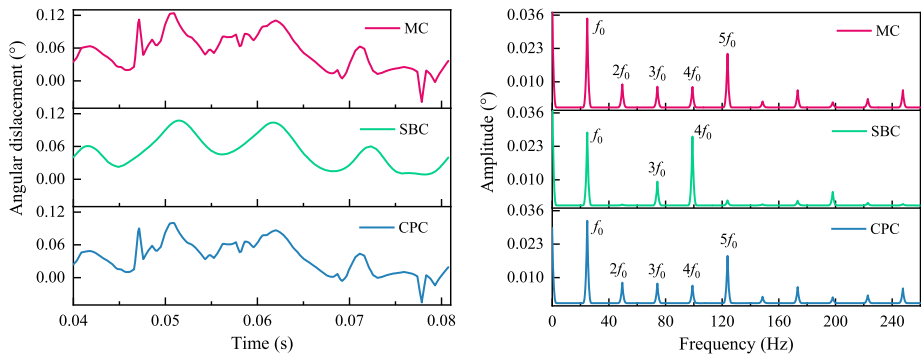
Fig. 15 Angular displacement of the crankshaft input end

the spindle necks. The stress distribution in MC follows a similar pattern to CPC, with both curves retaining noticeable nonlinear oscillation characteristics. The maximum stress occurs at 0.078 s, measuring 182.72 MPa, which is 15.53% lower than CPC. The stress distribution in MC is wider compared to CPC, but there is still evidence of stress concentration due to the influence of collision force. Overall, the stress comparison for the three cases is CPC > MC > SBC, indicating that the oil film support of the sliding bearing helps stabilize the shaft system and reduces stress concentration.

4.3.3 Crankshaft angular displacement analysis

The analysis of angular displacement in Fig. 15 shows that the time-domain curve for SBC is smoother because it does not consider the collision clearance at the crosshead pin. The amplitude of angular displacement is 0.107°, and the corresponding frequency-domain curve has fewer harmonics. Both MC and CPC consider the collision clearance, resulting in nonlinear oscillation characteristics in the time-domain curve. The trend of the angular displacement time-frequency curve for both conditions is in good agreement. The first five components of the fundamental frequency contribute to a certain extent. The amplitude of the CPC curve reaches 0.09°, while the corresponding amplitude of the MC curve is 23.82% higher than CPC, indicating a higher risk of resonance when considering CPC, while considering SBC helps reduce the risk of resonance.

4.4 Crankshaft system resonance analysis

During the operation of the compressor, the crankshaft system experiences alternating loads. In modal analysis, the load on the shafting can be converted into prestress, which impacts the structural stiffness and deformation of the crankshaft system, subsequently altering its natural frequency. Therefore, conducting modal analysis considering prestress is practically significant. Using the finite element method, prestressed modal analysis of the crankshaft system is performed under the conditions of CPC, SBC, and MC, respectively. The influence of different clearance parts on the torsional vibration of the shafting is compared and analyzed by examining the first 10-order prestressed modal frequencies and vibration modes for each clearance part. The details are shown in Table 4 and Fig. 16.

From Table 4, it can be observed that the natural frequencies of the crankshaft system in all three cases fall within the range of 370 Hz, and five modes of vibration occur, including

Table 4 Shafting modal information under different clearance parts

| Order	Crosshead pin clearance (CPC)		Sliding bear clearance (SBC)		Mixed clearance (MC)	
	Natural frequency/Hz	Mode of vibration	Natural frequency/Hz	Mode of vibration	Natural frequency/Hz	Mode of vibration
1	144.36	torsion	74.27	bending	73.25	bending
2	161.54	torsion	105.31	bending-torsion	80.32	bending-torsion
3	167.7	torsion	147.23	torsion	142.34	torsion
4	217.16	torsion	148.24	bending	149.08	bending
5	236.02	bending	188.62	bending	182.38	torsion
6	236.12	bending	192.34	torsion	193.43	bending
7	243.41	torsion	220.96	bending	220.96	bending
8	249.89	expansion	221.05	bending	221.05	bending
9	258.24	torsion	239.11	expansion	239.11	expansion
10	369.79	tension compression	241.15	tension compression	241.02	tension compression
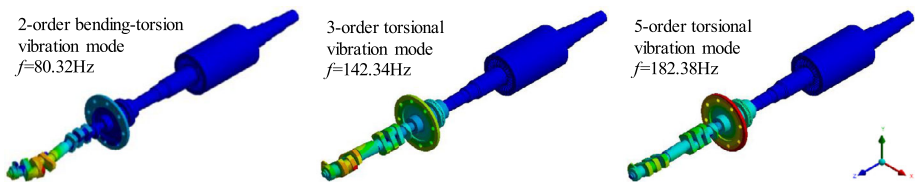
Fig. 16 Torsional and bending-torsional vibration modes of crankshaft system with mixed clearance

bending, torsion, bending and torsion, tension and compression, and expansion. The torsional modes and bending-torsional modes of the crankshaft system can be seen in Fig. 16.

When considering the CPC, the main journal is rigidly supported; it can be seen that the crankshaft system becomes less prone to bending, resulting in higher natural frequencies compared to the other cases. The first 10 natural frequencies under this condition range from 144.36 to 369.79 Hz. Torsional modes dominate, accounting for 60% of the first 10 modes.

When considering the SBC, the natural frequency of the shaft system is reduced due to the influence of oil film support at the main journal. The first 10 natural frequencies under this condition range from 74.27 Hz to 241.15 Hz, which are lower than those obtained under CPC. The first natural frequency in this scenario is 48.55% lower than that in the case of CPC. The reduced natural frequency indicates that the support stiffness of the shaft system decreases under the action of the oil film, resulting in a higher probability of bending deformation. This leads to the occurrence of bending and torsion modes after the superposition and coupling of torsional modes, which better aligns with engineering practice. Among these modes, the first 10 bending and torsion modes account for 30% and occur in the second, third, and sixth orders, while the bending mode dominates, accounting for 50% of the modes.

When considering the MC, the natural frequency of the crankshaft system is slightly lower than that of SBC, and the proportion of vibration mode is basically the same as that of SBC. However, torsion, bending, and torsion modes appear in the second, third, and fifth
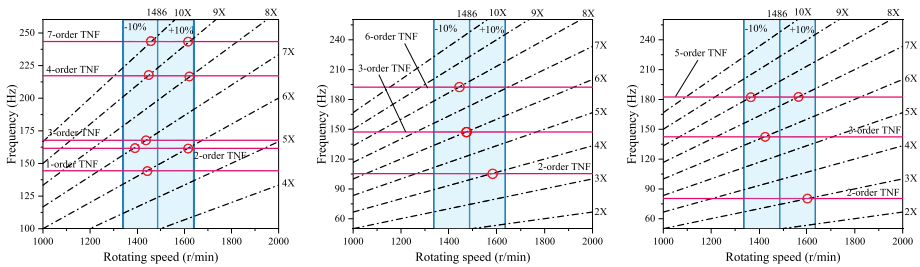
Fig. 17 Shafting resonance Campbell diagram (a) CPC model (b) SBC model (c) MC model

orders, and the frequency of torsion mode decreases. In general, under the same conditions, the CPC has little effect on the natural frequency and vibration mode of the shafting, while the SBC has a greater impact.

Based on the results of prestressed modal analysis, considering the API618 standard [63], which specifies limits for torsional natural frequencies (TNF) of crankshaft systems, the TNF should not fall within 10% of the upper and lower limits of the operating speed (1486 r/min), nor within 5% of any multiple of the speed below 10 times. To identify potential torsional resonance points of the shafting, the natural frequency of the torsional vibration is extracted, and a Campbell diagram is constructed for the crankshaft system under different clearance types, as shown in Fig. 16.

Figure 17 presents the Campbell diagram of the compressor crankshaft system resonance, with the horizontal line representing the critical speed and the oblique line indicating the resonance speed. Resonance occurs when the intersection point of these two lines falls within 10% of the upper and lower limits of the working speed (1486r/min). It can be seen from Fig. 17(a) that considering the CPC, there are 8 resonance points within the resonance speed range. On the other hand, Fig. 17(b) shows that considering the SBC, there are only 3 resonance points, greatly reducing the probability of resonance. The most practical scenario is observed in Fig. 17(c), where the MC is considered, and there are 4 resonance points. The corresponding operating speeds are 1367.8RPM, 1423.4RPM, 1563.3RPM, and 1606.4RPM. This demonstrates that collision nonlinearity increases the likelihood of torsional resonance, while the oil film support in SBC improves the smooth operation of the shaft system and reduces the risk of resonance. Therefore, a reasonable distribution of clearance composition contributes to the safe and stable operation of the crankshaft system.

5 Model validation

To verify the accuracy of the simulation model and results, we conducted a vibration test experiment on the crankshaft system under the same working conditions. We measured the dynamic torque of the compressor coupling to understand the torsional power transmission performance of the system. The compressor unit site is shown in Fig. 18.
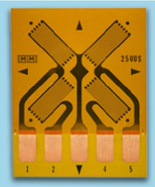
5.1 Experimental preparation and process

Due to the crankshaft system being sealed within the crankcase and inaccessible for disassembly, we selected measuring points on the coupling for the experiment. This ensured safety and feasibility and reduced the influence of airflow pulsation signals from the pipeline on the test results. The relevant test instruments and appliances used are listed in Table 5.

Fig. 18 Shale gas compressor site

Table 5 Main instrument of test

	TT10K-S wireless torque telemetry instrument	CEA-06-250USA-350 torque strain gauge	Surface cleaning agent	Strain gauge adhesive M-Bond 200 Kit
Test equipment				

The field test process is shown in Fig. 19.

The specific steps of the experiment process are as follows:

①. The measuring point on the motor shaft-coupling shaft section was polished with 320-mesh and 600-mesh sandpaper. Special oil removal and neutralizer agents for weak acid strain gauges were used to clean the area, ensuring a dust-free and stain-free surface.

②. The strain gauge pad was tinned with a soldering iron, and the strain gauge was aligned and installed with 3M non-constant tape on the measuring point.

③. The strain gauge was connected to the transmitter using a 4-core ribbon cable. The battery was also connected to the transmitter.

④. The transmitter was adjusted using a remote control and receiver to match the maximum input torque measurement range for the installed shaft diameter.

⑤. The compressor was started, and data acquisition commenced once the inlet and outlet pressure stabilized. The time-domain vibration velocity response data of the measuring point was recorded.

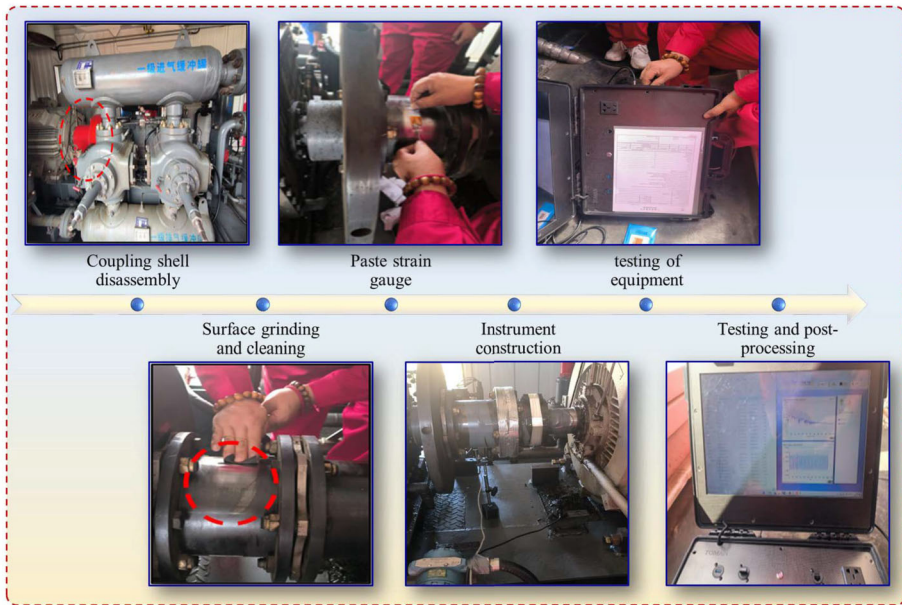⑥. Data processing involved eliminating unstable data and ensuring data continuity.

Fig. 19 Experimental process

5.2 Comparative analysis of test results

Stable data is extracted, and the experimental and simulation results are compared, as shown in Fig. 20. Overall, the variation pattern of the simulation and test results is similar. The maximum amplitude of the measured value is 3971.81 N m, while the maximum amplitude in the simulation is 3674.22 N m, resulting in an error of 7.49%, and the fluctuation of the experimental results is more obvious. The error can be attributed to the fact that the existence of more clearances, pipeline airflow pulsation, other moving equipment in the actual situation, and instrument accuracy. Nevertheless, the accuracy of the dynamic simulation calculation model of the crankshaft system, considering the mixed clearance, is verified within the acceptable range of the project.

6 Vibration reduction design of crankshaft clearance allocation

Combining the above analysis, it can be seen that there is a risk of torsional resonance in the shafting under MC; this section aimed to explore the torsional vibration mechanical response of the shafting under different combinations of CPC and SBC. Ultimately, we aimed to select fitting clearance that ensures stable transmission and minimizes the risk of torsional vibration. This guides the stable operation of the shafting.

6.1 Clearance configuration scheme design

Taking into account the oil supply pressure and operational reliability, three different gradient clearances of 0.07 mm, 0.1 mm, and 0.13 mm are selected as the new MC in the crankshaft system, SBC marked as A, B, and C, and CPC marked a, b, and c, as shown
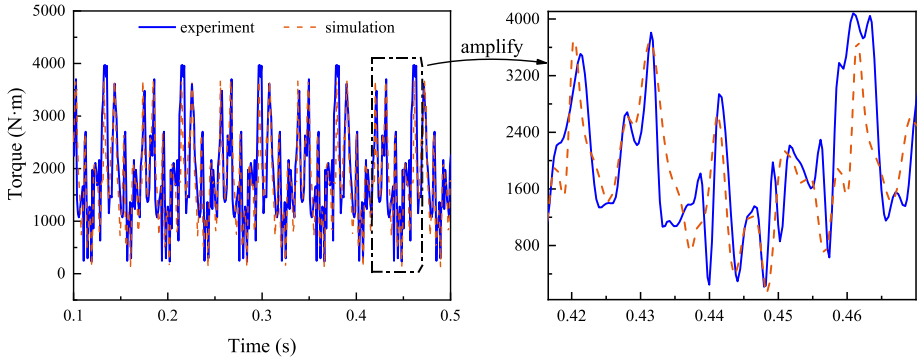
Fig. 20 Result contrast of experimental and simulation

Table 6 Clearance configuration of compressor crankshaft system

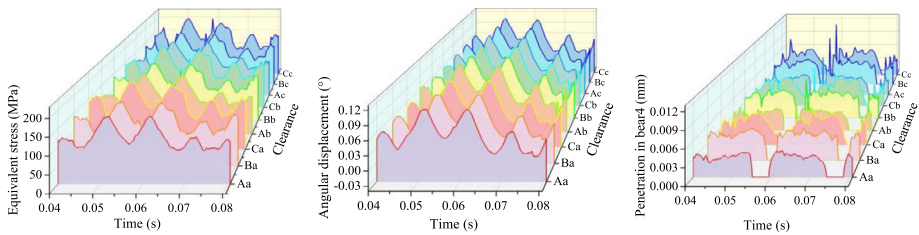| Crosshead pin clearance (CPC)	Sliding bearing clearance (SBC)		
	A–0.07	B–0.1	C–0.13
a–0.07	Aa	Ba	Ca
b–0.1	Ab	Bb	Cb
c–0.13	Ac	Bc	Cc

Fig. 21 Comparison of torsional vibration characteristics of shafting under different MC configurations

in Table 6. By analyzing the torsional vibration response under these clearances, a relatively appropriate clearance can be determined to ensure transmission stability and reduce torsional vibration risk.

6.2 Optimization of mixing clearance and comparison of vibration damping effect

Based on the analysis conducted, the study focuses on the dynamic stress distribution, angular displacement of the input end, and maximum rubbing amount of the shafting under different mixed clearances. These parameters are solved to quantitatively analyze the dynamic stability and matching of the shafting. The results, shown in Fig. 21, reveal that increasing the MC leads to obvious nonlinear characteristics in the stress and rubbing curves, while the angular displacement curve remains relatively unchanged. To further analyze the dynamic characteristics of the crankshaft system under different MCs, the peak stress, maximum angular displacement, and maximum rubbing amount are extracted and plotted in Fig. 22(a).
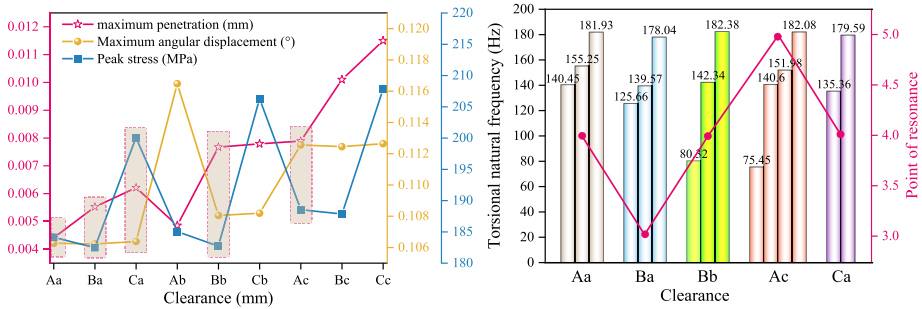
Fig. 22 Comparison of dynamic characteristics of different MCs. (a) Dynamic response peak of crankshaft system. (b) Torsional vibration frequency and resonance point of crankshaft system

From the trend in Fig. 22(a), it is apparent that these parameters do not increase with the clearance. Setting the mixed clearance to Ab results in the largest angular displacement of the input end, which is 0.128°, and lighter rubbing, indicating a larger torsional lag than other clearances of the shafting. Conversely, setting the clearance to Aa, Ba, or Ca, which corresponds to a minimum crosshead pin clearance of 0.07 mm, results in the smallest angular displacement. The corresponding crosshead pin clearance at this point should be avoided. On the whole, five relatively better results for Aa, Ba, Bb, Ac, and Ca can be selected. The prestressed modal analysis of the crankshaft system under these mixed clearances is carried out, and the torsional resonance probability of the shafting is judged in combination with the API 618 standard, as shown in Fig. 22 (b).

Figure 22(b) shows that Bb and Ac exhibit torsional vibration modes at low orders, while Ac has five torsional resonance points. This configuration places higher demands on the operation of the shafting and should be avoided. On the other hand, Ba has three torsional resonance points with relatively low risk. Additionally, the peak stress of the crankshaft system remains largely unchanged compared to the original scheme, while the maximum angular displacement is reduced by 1.76%, and the maximum rubbing amount is reduced by 29.49%. Therefore, a clearance configuration of 0.1 mm for the sliding bearing and 0.07 mm for the crosshead pin is a relatively better scheme, promoting smooth operation and effectively avoiding torsional resonance of the shafting.

7 Conclusions

This study focuses on the crankshaft system of a high-speed reciprocating compressor. It considers the influence of crosshead pin clearance, sliding bearing clearance, and flexible deformation of main force transmission components. The main contents and conclusions are as follows:

1. Based on Hertz's contact theory and multi-flexible body dynamics theory, a rigid-flexible coupling multibody dynamics model considering crosshead pin clearance is established. A forced vibration response analysis of the flexible crankshaft system with clearance was conducted. The analysis includes the motion accuracy of the crankshaft system, stability of shafting power transmission, and torsional matching of the shaft section. The results show that clearance greatly influences active acceleration, and the maximum error in acceleration is 400.1% compared with the ideal connection. The torque amplitude of the crankshaft end

increases by 5.88%, and the torque hysteresis increases, which aggravates the hysteresis performance of the crankshaft end torque and affects the transmission stability.

2. Dynamic characteristic coefficients of the sliding bearing are solved using the finite difference method and the pressure perturbation method. The bearing clearance constraint is modeled by the dynamic characteristic coefficient, and the collision force under the pin clearance is considered the boundary condition. The forced vibration response of the crankshaft system, considering mixed clearance, is solved using the finite element method. The dynamic characteristics and torsional resonance of the shafting under the three types of clearances of the crosshead pin clearance (CPC), the sliding bearing clearance (SBC), and the mixed clearance (MC) are compared and analyzed. The results show that under CPC, the angular displacement of the shaft system is 0.09°, the maximum equivalent stress of the shaft system is 216.26 MPa, and the first ten natural frequencies of the shaft system are higher compared to the other two clearances. When considering the CPC, the torsional resonance point is the most critical, with the highest risk of resonance. The risk of resonance is lower when considering the MC, and it is lowest when considering the SBC.

3. In order to verify the accuracy of the simulation results, the field vibration test of the compressor crankshaft system was carried out. Combined with the field conditions, the dynamic torque of the motor-coupling shaft section was measured. The simulation and experimental trends were basically the same, and the maximum error was 7.49%. Within the allowable range, the accuracy of the simulation results was effectively proved, which provided a basis for subsequent optimization.

4. A new MC scheme is proposed by combining different CPC and SBC configurations. The optimal clearance configuration for the shaft is analyzed, revealing that Ba, with a sliding bearing clearance of 0.1 mm and a crosshead clearance of 0.07 mm, is a relatively better scheme. This configuration reduces the maximum rubbing amount by 29.49% and the torsional resonance points from 4 to 3. Ultimately, it promotes the smooth operation of the shafting and effectively avoids torsional resonance.

Declarations

References

1. Soong, K., Thompson, B.S.: A theoretical and experimental investigation of the dynamic response of a slider-crank mechanism with radial clearance in the gudgeon-pin joint. J. Mech. Des. **112**(2), 183–189 (1990)
2. Flores, P., Ambrósio, J., Claro, J.P.: Dynamic analysis for planar multibody mechanical systems with lubricated joints. Multibody Syst. Dyn. **12**(1), 47–74 (2004)
3. Erkaya, S., İbrahim, U.: Experimental investigation of joint clearance effects on the dynamics of a slider-crank mechanism. Multibody Syst. Dyn. **24**(1), 81–102 (2010)

4. Muvengei, O., Kihiu, J., Ikua, B.: Dynamic analysis of planar rigid-body mechanical systems with two-clearance revolute joints. Nonlinear Dyn. **73**(1), 259–273 (2013)

5. Zhao, B., Zhou, K., Xie, Y.B.: A new numerical method for planar multibody system with mixed lubricated revolute joint. Int. J. Mech. Sci. **113**, 105–119 (2016)

6. Flores, P., Ambrósio, J., Claro, J.C.P., Lankarani, H.M., Koshy, C.S.: A study on dynamics of mechanical systems including joints with clearance and lubrication. Mech. Mach. Theory **41**(3), 247–261 (2006)

7. Brutti, C., Coglitore, G., Valentini, P.P.: Modeling 3D revolute joint with clearance and contact stiffness. Nonlinear Dyn. **66**(4), 531–548 (2011)

8. Marques, F., Isaac, F., Dourado, N., et al.: An enhanced formulation to model spatial revolute joints with radial and axial clearances. Mech. Mach. Theory **116**, 123–144 (2017)

9. Liu, T.S., Qian, L.F., Yin, Q.: Kinematics accuracy and dynamic analysis of multibody systems with spatial cylindrical clearance joints. J. Vib. Shock **36**(19), 151–157 (2017)

10. Bai, Z.F., Zhao, J.J., Zhao, Y.: Dynamic analysis of mechanical system considering radial and axial clearances in 3D revolute clearance joints. J. Vib. Control **27**, 1893–1909 (2021)

11. Zhao, Y., Bai, Z.F.: Dynamics analysis of space robot manipulator with joint clearance. Acta Astronaut. **68**, 1147–1155 (2011)

12. Zhang, X.C., Zhang, X.M., Chen, Z.: Dynamic analysis of a 3-RRR parallel mechanism with multiple clearance joints. Mech. Mach. Theory **78**, 105–115 (2014)

13. Chen, Y., Sun, Y., Yang, D.: Investigations on the dynamic characteristics of a planar slider-crank mechanism for a high-speed press system that considers joint clearance. J. Mech. Sci. Technol. **31**(1), 75–85 (2017)

14. Yan, S., Xiang, W., Zhang, L.: A comprehensive model for 3D revolute joints with clearances in mechanical systems. Nonlinear Dyn. **80**, 309–328 (2015)

15. Chen, Y., Feng, J., Peng, X., Sun, Y., He, Q., Yu, C.T.: An approach for dynamic analysis of planar multibody systems with revolute clearance joints. Eng. Comput. **37**(3), 2159–2172 (2020)

16. Bai, Z.F., Liu, T., Li, J.Y., Zhao, J.J.: Numerical and experimental study on dynamic characteristics of planar mechanism with mixed clearances. Mech. Based Des. Struct. Mach. **51**(11), 1–24 (2022)

17. Morita, T., Okamura, H.: Simple modeling and analysis for crankshaft three-dimensional vibrations, Part2: application to an operating engine crankshaft. J. Vib. Acoust. **117**(1), 80 (1995)

18. Kimura, J., Shiono, K., Okamura, H.: Experiments and analysis of crankshaft three-dimensional vibrations and bending stress in a V-type ten-cylinder engine: influence of crankshaft gyroscopic motions SAE Pap. **106**, 971995 (1997)

19. Nestorides, E.J.: A Handbook on Torsional Vibration. Cambridge University Press, London (1958)

20. Xu, L., Li, Y., Li, C., Yang, Y.: Effects of bearing clearance and flexibility on the dynamic errors of mechanisms. J. Mech. Eng. **48**(7), 30–36 (2012)

21. Lai, T.W., Chen, S.T., Ma, B., Zheng, Y.Q., Hou, Y.: Effects of bearing clearance and supporting stiffness on performances of rotor-bearing system with multi-decked protuberant gas foil journal bearing. Proc. Inst. Mech. Eng., Part J J. Eng. Tribol. **228**(7), 780–788 (2014)

22. Smolík, L., Hajžman, M., Byrtus, M.: Investigation of bearing clearance effects in dynamics of turbochargers. Int. J. Mech. Sci. **127**, 62–72 (2017)

23. Li, S.T.: A mathematical model and numeric method for contact analysis of rolling bearings. Mech. Mach. Theory **119**, 61–73 (2018)

24. Xu, H.Y., Ma, H., Wen, B.G., Yang, Y., Li, X.P., Luo, Z., Han, Q.K., Wen, B.C.: Dynamic characteristics of spindle-bearing with tilted pedestal and clearance fit. Int. J. Mech. Sci. **261**, 108683 (2023)

25. Chen, K.X., Wang, D.W., Dong, X.W.: Study on the influence of sliding bearing radial clearance on the rotor system vibration characteristics. Mach. Tool Hydraul. **50**(14), 131–135 (2022)

26. Wei, W., Guo, W.Y., Wu, X.Y.: Stability analysis on sliding bearing with consideration of clearance. Lubr. Eng. **43**(10), 18–22 (2018)

27. Ma, B.A., Khemili, I., Aifaoui, N.: Numerical investigation of a flexible slider-crank mechanism with multi-joints with clearance. Multibody Syst. Dyn. **38**(2), 173–199 (2016)

28. Li, Y.Y., Chen, G.P., Sun, D.Y., Gao, Y., Wang, K.: Dynamic analysis and optimization design of a planar slider-crank mechanism with flexible components and two clearance joints. Mech. Mach. Theory **99**, 37–57 (2016)

29. Yao, T.Q., Chen, R.B., Wang, L.H.: Flexible multibody dynamics analysis method of spatial mechanisms considering 3-D cylindrical hinges clearance collision. J. Vib. Shock **40**(01), 297–307 (2021)

30. Chen, X.L., Jiang, S., Deng, Y., Wang, Q.: Dynamics analysis of 2-DOF complex planar mechanical system with joint clearance and flexible links. Nonlinear Dyn. **93**(3), 1009–1034 (2018)

31. Zheng, E.L., Wang, T.Y., Guo, J., Zhu, Y., Lin, X.Z., Wang, Y.J., Kang, M.: Dynamic modeling and error analysis of planar flexible multilink mechanism with clearance and spindle-bearing structure. Mech. Mach. Theory **131**, 234–260 (2019)

32. Bauchau, O., Rodriguez, J.: Modeling of joints with clearance in flexible multibody systems. Int. J. Solids Struct. **39**(1), 41–63 (2002)
33. Khemili, I., Romdhane, L.: Dynamic analysis of a flexible slider–crank mechanism with clearance. Eur. J. Mech. A, Solids **27**(5), 882–898 (2008)
34. Xu, L.X., Yang, Y.H., Li, Y.G., Li, C.N.: Modeling and analysis of planar multibody systems containing deep groove ball bearing with clearance. Mech. Mach. Theory **56**, 69–88 (2012)
35. Zhao, B., Zhang, Z.N., Dai, X.D.: Modeling and prediction of wear at revolute clearance joints in flexible multibody systems. Proc. Inst. Mech. Eng., Part C, J. Mech. Eng. Sci. **228**(2), 317–329 (2014)
36. Ebrahimi, S., Salahshoor, E., Moradi, S.: Vibration performance evaluation of planar flexible multibody systems with joint clearance. J. Braz. Soc. Mech. Sci. Eng. **39**(12), 4895–4909 (2017)
37. Zheng, E.L., Zhou, X.L.: Modeling and simulation of flexible slider-crank mechanism with clearance for a closed high speed press system. Mech. Mach. Theory **74**, 10–30 (2014)
38. Dong, X.Y., Sun, Y., Wu, X.Z., et al.: Dynamic modeling and performance analysis of toggle-linkage presses considering mixed clearances and flexibility. Int. J. Non-Linear Mech. **147**, 104243 (2022)
39. Wang, G.X., Wang, L.: Dynamics investigation of spatial parallel mechanism considering rod flexibility and spherical joint clearance. Mech. Mach. Theory **137**, 83–107 (2019)
40. Tian, Q.A., Liu, C., Machado, M., et al.: A new model for dry and lubricated cylindrical joints with clearance in spatial flexible multibody systems. Nonlinear Dyn. **64**, 25–47 (2011)
41. Ma, Z.D., Perkins, N.C.: An efficient multibody dynamics model for internal combustion engine systems. Multibody Syst. Dyn. **10**(4), 363–391 (2003)
42. Du, H.Y.I.: Simulation of flexible rotating crankshaft with flexible engine block and hydrodynamic bearings for a V6 engine. SAE Transact. **108**, 1852–1860 (1999)
43. Chen, L., Song, X., Xue, D.X., Ming, Z.J.: Elastohydrodynamic lubrication and asperity contact simulation of engine main bearing with flexible rotating crankshaft and flexible engine block. In: Advanced Tribology, pp. 967–972 (2010)
44. Wei, L.D.: Thermo-elasto-hydrodynamic mixed lubrication of main bearings of marine diesel engines, based on coupling between flexible engine block and crankshaft. J. Mech. Eng. **50**, 97–105 (2014)
45. Xu, Y.M., Teng, X.B., Yu, Z.M.: Multibody dynamics analysis of V-type diesel engine crankshaft. Open Mech. Eng. J. **8**, 744–749 (2014)
46. Zhou, W., Liao, R.: Dynamic characteristic based on modal superposition method and structure optimization of crankshaft. Trans. Chin. Soc. Agric. Eng. **31**(3), 129–136 (2015)
47. Wang, M.S., Xiao, N.Q., Fan, M.H.: The torsional vibration simulation of the diesel engine crankshaft system based on multibody dynamic model. J. Multibody Dyn. **235**(3), 443–451 (2021)
48. Qin, W.J., Jia, D.W., Liu, Q.Y.: Multibody system dynamics simulation of loads in main bearings of crankshafts. Mater. Sci. Forum **628**(629), 55–60 (2009)
49. Drab, C.B., Engl, H.W., Haslinger, J.R., Offner, G., Pfau, R.U., Zulehner, W.: Dynamic simulation of crankshaft multibody systems. Multibody Syst. Dyn. **22**(2), 133–144 (2009)
50. Lv, J.H., Chu, Y.X., Feng, Z.M.: Rigid and flexible coupling analysis of crankshaft system. In: Proceedings of the 8th International Conference on Social Network, Communication and Education (SNCE 2018) (2018)
51. Nowakowski, C., Kürschner, P., Eberhard, P., et al.: Model reduction of an elastic crankshaft for elastic multibody simulations. Z. Angew. Math. Mech. **93**(4), 198–216 (2013)
52. Bai, Z.F., Zhao, Y., Zhao, Z.G.: Dynamic characteristics of mechanisms with joint clearance. J. Vib. Shock **30**(11), 17–20, 41 (2011)
53. Xue, Z.P., Zhang, H., Dynamic, J.Y.G.: Response of a flexible multibody in large wind turbines: a review. Sustainability **15**, 6590 (2023)
54. Zhang, X., Zheng, L.: Investigation on the dynamics of a flexible multibody system of a three-cylinder gasoline engine crankshaft. Processes **11**(1248), 1248 (2023)
55. Bernd, S.: On Lagrange multipliers in flexible multibody dynamics. Comput. Methods Appl. Mech. Eng. **195**, 6993–7005 (2006)
56. Xiang, W.K., Yan, S.Z., Wu, J.N.: Complexity evaluation of nonlinear dynamic behavior of mechanisms with clearance joints by using the fractal method. Proc. Inst. Mech. Eng., Part C, J. Mech. Eng. Sci. **228**(18), 3482–3495 (2014)
57. Craig, R.R., Brampton, M.C.C.: Coupling of substructures for dynamics analysis. AIAA J. **6**, 1313–1319 (1968)
58. Craig, R.R.: A review of time-domain and frequency-domain component mode synthesis method. Comb. Exp. Anal. Model. Dyn. Struct. Syst. **12**(3), 1–30 (1985)
59. Wang, X.P., Liu, G., Ma, S.J.: Effects of clearance joint on impact dynamic characteristics of planar mechanisms. J. Vib. Shock **36**(17), 74–78 (2017)
60. Zhou, Y.J., Guan, F.L.: Dynamics analysis of mechanisms with elastic bars and three-dimensional clearance revolute joints. J. Harbin Inst. Tech. **44**, 122–127 (2016)

61. Wei, L.D., Wei, H.J., Duan, S.L.: An EHD-mixed lubrication analysis of main bearings for diesel engine based on coupling between flexible whole engine block and crankshaft. Ind. Lubr. Tribol. **67**(2), 150–158 (2015)
62. Wen, B.C., Gu, J.L., Xia, S.B., et al.: Advanced Rotor Dynamics: Theory, Technology and Application, pp. 80–89. Mechanical Industry Press, Beijing (2000)
63. American Petroleum Institute: Reciprocating compressors for petroleum chemical and gas industry service: AP1 618. Washington D C: American Petroleum Institute (2007)